Spatio-temporal characterization of slope damage: insights from the Ten Mile Slide, British Columbia, Canada

Spatio-temporal characterization of slope damage: Insights from the Ten Mile Slide, British Columbia, Canada

Davide Donati [1]* (davide_donati@sfu.ca; ORCiD: 0000-0003-4083-5910); Doug Stead [1] (dstead@sfu.ca); Matthew Lato [2] (mlato@bgcengineering.ca), Sarah Gaib[3] (sarah.gaib@gov.bc.ca)

1 Dept. of Earth Sciences, Simon Fraser University, Vancouver, Canada

2 BGC Engineering, Vancouver, Canada

3 BC Ministry of Transportation and Infrastructure, Victoria, BC, Canada

* Corresponding author:

Davide Donati - Dept. of Earth Sciences - Simon Fraser University - Vancouver, Canada

email: davide_donati@sfu.ca; phone: +1 (778) 782-4165

Abstract

The deformation and failure of slopes is associated with the formation of geomorphic features reflecting "external slope damage". Characterizing the spatial and temporal distribution of slope damage is beneficial to understanding the mechanisms and processes underlying slope instability. To date, characterization of slope damage has predominantly been performed using qualitative approaches. In this paper, a new workflow for the quantitative, spatio-temporal characterization of the external slope damage is described and applied to the investigation of the Ten Mile Slide, an active landslide located in southern British Columbia. Since 2006, monitoring activity at the site has included periodic repeat airborne laser scanning (ALS) surveys, which have allowed the creation of a high-detail, three-dimensional database showing the progressive deformation and retrogression of the slide. External slope damage features are manually mapped in the ALS datasets, and slope damage intensity is then computed and displayed on thematic maps. The proposed workflow introduces important new slope damage measures including External Discrete Slope Damage Feature maps (EDSDF), External Slope Damage Intensity Cell (ESDICe) maps, External Slope Damage Intensity Contour (ESDICo) maps and slope Damage intensity spatio-temporal plots. The new spatio-temporal damage measures are used to create damage index tables and track changes in slope damage intensity with time at any point within the slide area. The spatio-temporal analysis shows that the distribution of external slope damage features is not homogeneous across the Ten Mile Slide area. In particular, the spatio-temporal damage methodology outlines higher

accumulation slope damage rates along the eastern boundary of the slide area, due to the presence of a stream incision that provides kinematic freedom and allows the lateral deformation of the slide and the formation of tensile cracking. The proposed approach in this thesis allows comprehensive, quantitative, and repeatable damage analysis to be undertaken, providing a robust method for characterizing the geomorphic evolution of slopes from a damage perspective. This research methodology provides engineers and geoscientists with a valuable tool for planning subsequent slope investigation and optimizing new or existing monitoring and early-warning systems.

Keywords: Slope damage; slope stability; Ten Mile Slide; remote sensing; ALS.

1 Introduction

The stability of rock slopes is controlled by numerous factors. Tectonic structures, such as faults, folds, and joints, may act as rear and lateral release surfaces, and provide kinematic freedom for the detachment of rock slides (Brideau and Stead, 2011). Structural and lithological features, such as foliation, cleavage, and bedding planes, may provide slope failures with a basal rupture surface, due to their typically high persistence (Stead and Wolter, 2015). Endogenic and exogenic factors, such as earthquakes, heavy rainfall events, and cyclic groundwater fluctuations, progressively weaken the slope, inducing deformations and driving progressive slope failure (Gischig et al., 2015; Preisig et al., 2016).

The gradual deformation of a slope results in the accumulation of slope damage (Stead and Eberhardt, 2013). Several authors have analyzed slope damage features that developed at various landslides, to identify the factors, processes, and mechanisms governing the evolution of a slope. Chigira (1992) described the ductile and brittle deformation occurring in rock slopes affected by "mass rock creep" (MRC), highlighting the role of lithological characteristic of the rock mass, such as bedding orientation, and the slope morphology. Agliardi et al. (2001) analyzed the geomorphic features (double-ridges, scarps, counterscarps, and grabens) commonly associated with the development of deep-seated gravitational slope deformations (DSGSDs). Fell et al. (2007) and Glastonbury and Fell (2008) reviewed several rockslides, briefly summarizing slope damage features associated with various types of movement. Jaboyedoff et al. (2013) provided a review of the structures and features that form during the gravitational deformation of rock slopes addressing the importance of inherited structures and past deformation events. Agliardi et al. (2013) investigated the rock mass damage and structures that developed within an unstable quarry wall as a result of ongoing slope deformation. Havaej et al. (2014) employed a numerical modelling approach to conceptually investigate the importance of brittle damage in the failure of bi-planar slides. Traditional field work, site reconnaissance, and photogrammetric analyses have been largely relied on for the investigation of rock slope instabilities and damage features (Mathews and McTaggart, 1969; Piteau et al., 1978). More recently, technological advancements in remote sensing techniques have greatly enhanced the ability to comprehensively characterize rock slopes (Donati et al., 2017). Research by Westin (2017) and Francioni et al. (2018) are useful examples of the benefits that remote sensing techniques (and in particular ALS datasets) may provide in the investigation of rock slopes and slope damage, compared to an exclusively field-based approach.

Investigating how the spatial distribution of slope damage within a landslide changes with time is fundamental in understanding the evolution of a slope and the factors controlling stability. Clayton et al. (2017) analyzed the progressive accumulation of damage at the Mitchell Creek slide, in northern British Columbia. They characterized the geomorphic evolution of the slope using four sets of aerial photographs, observing that instability at the site was driven by the retreat of the glacier in the valley below. Scarps, counterscarps, and tension cracks were identified as the main evidence of ongoing deformation. Roberti et al. (2018) qualitatively investigated the geomorphic evolution of the volcanic slopes of Mount Meager. They observed that the progressive glacier retreat resulted in the formation of slope damage features (counterscarps and tension cracks), up until the catastrophic failure that occurred in 2010.

The use of high-frequency terrestrial laser scanner (TLS) monitoring has also been successfully applied for the analysis of unstable rock slopes. Kromer et al. (2015) investigated the evolution of an unstable slope along the White Canyon in the Fraser River Valley (British Columbia) prior to and after the failure of a 2,300 m^3 rockslide in 2013. They observed a progressive increase in rockfall volume and frequency in the months before the failure and concluded that the investigation of precursory events is a key step in the hazard analysis in transportation corridors. Williams et al. (2018) employed a near-continuous monitoring approach to spatially and temporally quantify the rockfalls detaching from a sea cliff in Whitby (UK), and developed an optimized workflow for the analysis of high-frequency and high-resolution datasets.

In this paper, we quantitatively characterize the accumulation of rock slope damage at the Ten Mile Slide, an unstable slope located in southern British Columbia (Canada). The objective is to identify the potential factors controlling the spatial variation of slope damage intensity and accumulation rates. Slope monitoring activity at the Ten Mile Slide has included the collection of extensive high-resolution ALS datasets collected periodically between 2006 and 2017. A GIS approach is developed that allows the mapping and characterization of discrete damage features, and the creation of damage intensity maps describing the spatial distribution of slope damage. Finally, the processed thematic maps are used to investigate the evolution with time of the slope damage.

2 The Ten Mile Slide

2.1. Geographic, geological, and geomorphic overview

The Ten Mile Slide is located in southern British Columbia (Canada), approximately 8 km north-east of the town of Lillooet (Figure 1a). The slide affects the left, southern bank of the Fraser River valley and formed within the boundaries of a post-glacial landslide known as the Tunnel earthflow (Bovis, 1985). Since its reactivation in 1984 (Hensold et al., 2017), the slide evolution has been causing the displacement and deformation of two major infrastructures that cross the slide area, Highway 99 and the Canadian National Railway (CN) track (Figure 1b).

The bedrock in the slide area comprises volcanic materials, including Eocene and Cretaceous lava flows (basalt to rhyolite, and andesite to dacite, respectively), and sedimentary successions (sandstone, conglomerate, and shale) of the Jackass Mountain group (Bovis, 1985). Tectonic structures crossing the investigated area are predominantly oriented in a north-south direction, and form part of the Fraser River Fault System, which extends for 80 km to the south, towards the area of Hope (British Columbia, Canada) (Monger and McMillan, 1984).

The major geomorphic element within the investigated area is the Fraser River, which flows from east to west at the base of the slope, at an elevation of 225 m. The slope extends to a maximum elevation of about 1,010 m, whereas the vertical extent of the slide is limited to between elevations 250 m and 400 m. The slope in the slide area dips towards the northwest with an average slope angle of 24°, which increases to 42° in the lower part, below the highway. The slide is bounded, on the eastern side, by a gully that is particularly prominent in the upper slope (Figure 1b).

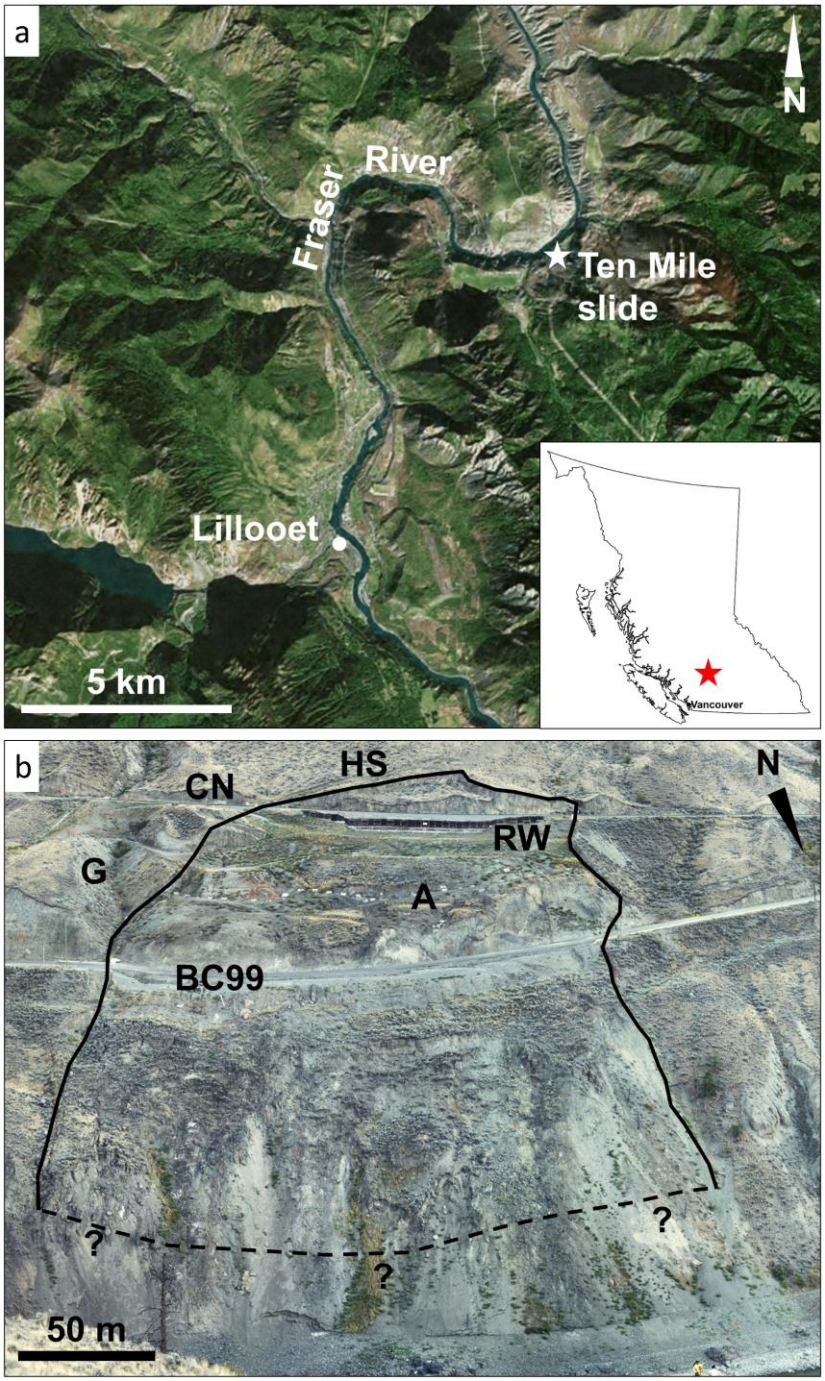

Figure 1: Overview of the investigated area. a: 2005 satellite image of the Fraser River Valley North of Lillooet. The star indicates the location of the Ten Mile Slide, on the left bank of the Fraser River. In the inset, the star indicates the location of the slide area in British Columbia, Canada; b: 2017 panoramic photograph of the slide area, outlined in black. HS: headscarp; CN: Canadian National Railway; RW: retaining wall; G: gully; A: anchor line; BC99: British Columbia Highway 99.

The landslide extends for 250 m in the north-south direction (i.e., downslope), and 190 m in the east-west direction (i.e., across slope), covering an area of about 4.1 x 10^4 m^2. Over 30 boreholes have been drilled within the

slide area, and the thickness of the landslide found to vary between 10 and 30 m (Hensold et al., 2017). The slide volume was estimated at between 0.75 and 1 million m^3 (Macciotta et al., 2016), predominantly comprising landslide material (including medium to high plasticity clay, with layers of sands and gravel), overlying colluvium and glacial deposits. The slide is currently moving along a continuous rupture surface sub-parallel to the slope (Hensold et al., 2017). The slide initiated in the lower slope, 40 to 80 m below the highway, and has gradually retrogressed at an increasing rate until it reached its current extent (Hensold et al., 2017). The displacement is mainly driven by the creeping behavior of the slide material with contributions of anthropogenic activity, whereas groundwater pressure does not have a significant role on the slide behavior (Carlà et al., 2017). Limit equilibrium analyses indicated that a Factor of Safety of 1 exists along the sliding surface if a friction angle of 21° is considered (Hensold et al., 2017).

2.2. Slope monitoring and stabilization measures

Slope displacement has been monitored for over thirty years. Historical displacement rates of 5-8 mm/day have been observed along the highway (Hensold et al., 2017), and initial remedial measures were directed to realigning the highway to counter the gradual downslope displacement. In 2007, slope deformation was observed at the railway track, which had been previously largely unaffected by the slide. This development triggered the installation of a retaining wall below the CN railway (Hensold et al., 2017). In 2011, a trench drain was also built to divert surface water away from the slide area, and a row of shear key panels was installed along the highway. After an initial decrease, displacement rates increased back to pre-remediation values in 2013 (Hensold et al., 2017).

Between 2014 and 2015, displacement rates of 6 mm/day and 10 mm/day were observed along the CN track and the highway, respectively. In an attempt to slow down the slide, 253 micro-piles and grouted strand anchors were installed, in 2016, between the highway and the railway, and within the existing retaining wall (Carlà et al., 2017; Hensold et al., 2017). Displacement rates increased to 25 mm/hr at the end of September 2016, triggering the closure of the highway for eight days due to safety concerns (Hensold et al., 2017). In response to this acceleration, a row of 30 anchors was installed, in winter 2017, throughout the full width of the slide area at an elevation of 330 m (Carlà et al., 2017; Hensold et al., 2017). After the installation of remedial works displacement rates decreased above the highway and have almost stopped above the CN track. However, the lower slope remains active (Hensold et al., 2017).

On site monitoring systems include borehole inclinometers, survey targets, geometry measurements along the CN railway track (Macciotta et al., 2017, Hensold et al., 2017) and, more recently, a GPS system (Carlà et al., 2017). Monitoring also involves the use of ALS surveys that have been performed periodically since 2006. This monitoring activity has allowed for the collection of a large dataset that describes in detail the progressive deformation of the Ten Mile Slide. From the investigation of the ALS datasets it was possible to perform change detection analyses that show, between 2006 and 2016, negative changes (i.e., a decrease in ground elevation) in the upper part of the slope and positive changes (i.e., an increase in ground elevation) in the lower slope (above and below elevation 330 m, respectively, Lato et al. 2016). Additionally, the ALS investigation allowed for the sub-division of the slide into 19 blocks, the displacement rate and direction of which were investigated using roto-translational analyses (Lato et al., 2016)

3 Research methodology

3.1. Suggested slope damage descriptors

The characterization of slope damage requires a reliable set of descriptors that allow damage features to be classified based on their location, spatial distribution, and origin. Stead and Eberhardt (2013) suggested that slope damage could be considered as "internal" and "external", depending on whether or not the features are visible at the slope surface. Typically, external slope damage features can be investigated using remote sensing techniques and traditional field mapping. Conversely, the characterization of internal slope damage requires the use of sub-surface datasets that can only be obtained from borehole drilling or geophysical methods. Slope damage may also be described and classified based on the areal/subsurface distribution of damage as "focused" or "distributed". Finally, slope damage may be distinguished between "tensile" and "shear", depending on the mechanism of failure. Throughout this research, the aforementioned descriptors are used to qualitatively describe single features observed during the field reconnaissance, and in the ALS datasets. However, at this stage, no attempt is made to perform a systematic classification of the slope damage features mapped in the ALS datasets.

3.2. Quantitative slope damage characterization at the Ten Mile Slide

The spatio-temporal investigation of slope damage at the Ten Mile Slide involved the analysis, mapping, and comparison of the various ALS datasets made available by the Ministry of Transportation and Infrastructure of British Columbia. Aspect, slope, and hillshade maps were created for each dataset, using the respective tools in ArcGIS 10.5 (ESRI, 2017). Discrete slope damage features were then manually mapped as polylines after visually inspecting the maps. Manual mapping of slope damage features clearly can represent a source of subjectivity, as different users may give different interpretation of the same feature, potentially resulting in differences in computed slope damage intensity. To minimize subjectivity, semi-automated mapping approaches may be implemented in the workflow (e.g., Stumpf et al., 2013; Leshchinsky, 2016; de Vilder et al., 2017). The application of semi-automated mapping techniques to produce EDSDF maps will be tested in future analyses. Additionally, we emphasise that the presented approach can only consider slope damage features that are visible at the slope surface at the time of the survey (i.e., ALS flights). Therefore, it is important to address and consider the action of anthropic and natural processes that, by acting at the slope surface, may reduce the visibility of slope damage, by infilling or covering discrete features, thus affecting the mapping accuracy, regardless of the method employed. The impact of this limitation can be potentially reduced by increasing the frequency of the surveys, thus allowing for an improved correlation between the timing of significant natural or anthropic events (e.g., heavy rainfall, slope regrading, excavations, etc.) and sudden variations in slope damage feature distribution.

In order to assess the distribution of slope damage throughout the slide area, a slope damage intensity approach was used. The concept of slope damage intensity (SD_{21}) is derived from the fracture intensity (P_{21}), a parameter used in rock engineering practice for the construction of Discrete Fracture Networks (Dershowitz et al., 2000). SD_{21} is defined as the total length of slope damage traces per unit area and is measured in m^{-1}.

Slope damage analysis at the Ten Mile Slide was performed by dividing the slide area into equidimensional cells, in which a value of SD_{21} was computed using the cumulative length of the damage features mapped within each cell. To provide the reader with a "reference frame" for the interpretation of the SD_{21} values, Figure 2 shows the values calculated for 9 cells in the November 2015 ALS dataset. The coordinates of the central point of the cell and the relative SD_{21} value were then exported and interpolated in Surfer 14 (Golden Software, 2016), using a Kriging method, to create a spatial damage intensity map. SD_{21} maps were built for each ALS temporal dataset, in order to assess the evolution in slope damage distribution. Various map types were developed to visualize the spatial distribution of slope damage: External Discrete Slope Damage Features maps (EDSDF), External Slope Damage Intensity Cell maps (ESDICe), and External Slope Damage Intensity Contour maps (ESDICo). Figure 3 summarizes procedure developed in this study for the spatio-temporal analysis of slope damage at the Ten Mile Slide site.

3.2.1. External Discrete Slope Damage Features (EDSDF) maps

An EDSDF map displays all the observed slope damage features, mapped as polylines in the examined datasets. EDSDF maps allow the user to investigate geometrical parameters such as damage feature persistence and orientation.

3.2.2. External Slope Damage Intensity Cell (ESDICe) maps

An ESDICe map is a color-coded representation of each SD_{21} cell, which can represent either the absolute or normalized value of slope damage intensity. This type of visualization method allows for the quantitative comparison of multiple temporal datasets. The results are dependent on the selected cell size. Small cells will cause the damage intensity to sharply increase or decrease, depending on whether a feature intersects a cell or not. Very small cells would cause the ESDICe map to be similar to an EDSDF map. Conversely, large cells will cause a loss of detail, as the damage feature length is distributed over wide areas that potentially include relatively undamaged parts of the slope. The ideal selected cell size is site-dependent and should provide the best detail using the largest cell surface area.

3.2.3. External Slope Damage Intensity Contour (ESDICo) maps

ESDICo maps are created by interpolating points at the centre of the cells within which SD_{21} values are computed. While in the case of ESDICe maps the cells cannot overlap, due to the color-coded nature of the representation, cells used to create ESDICo maps can overlap to increase the number of points available for the interpolation, providing a smoother transition between cells throughout the investigated area.

3.2.4. Damage intensity time plots

An approach for investigating temporal evolution of SD_{21} at specified locations was developed. The SD_{21} values of each cell and for each ALS dataset are imported into an indexed table, which can be interrogated using a Python script. As the SD_{21} value for each cell is estimated at different times, its value can be plotted to graphically visualize the variation of slope damage intensity with time.

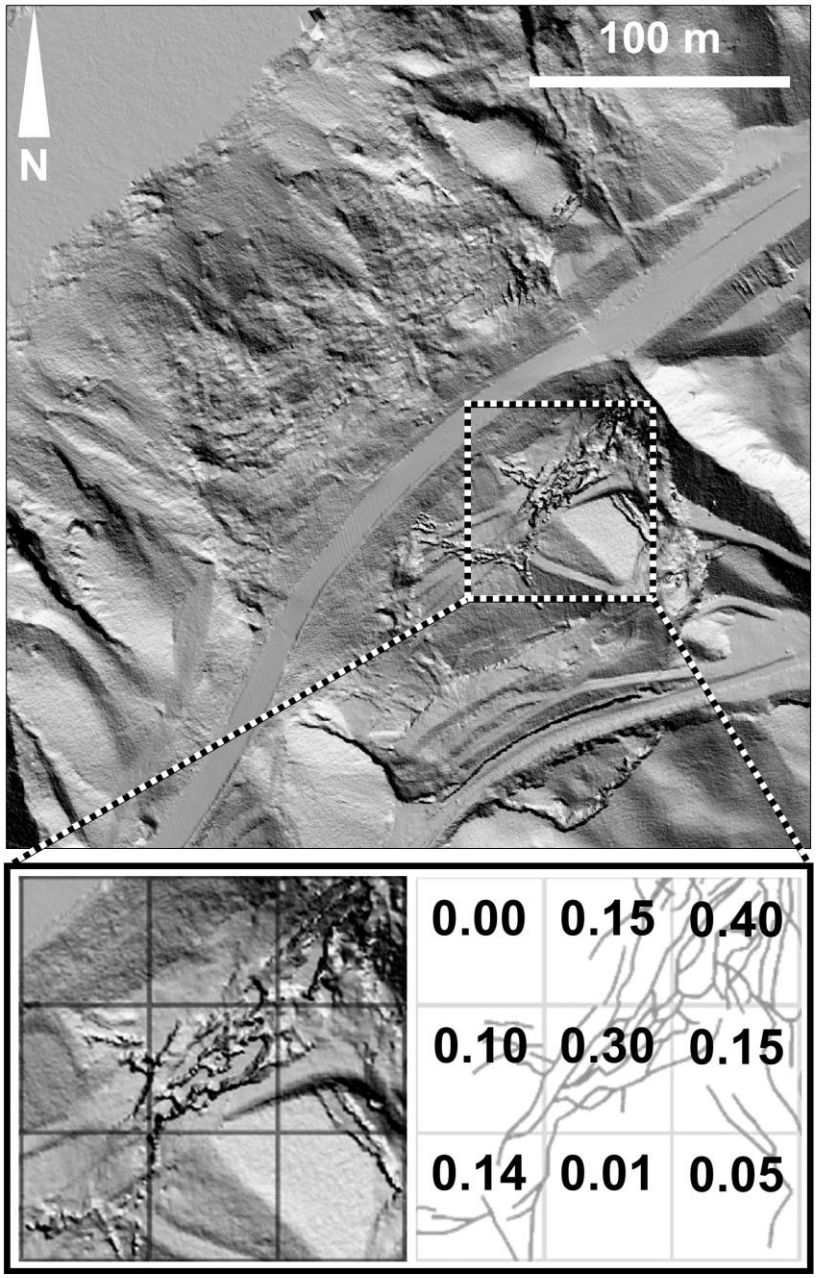

Figure 2: Example of the SD_{21} values calculated for 9 quadrangular cells (25 m x 25 m) within the November 2015 ALS dataset.

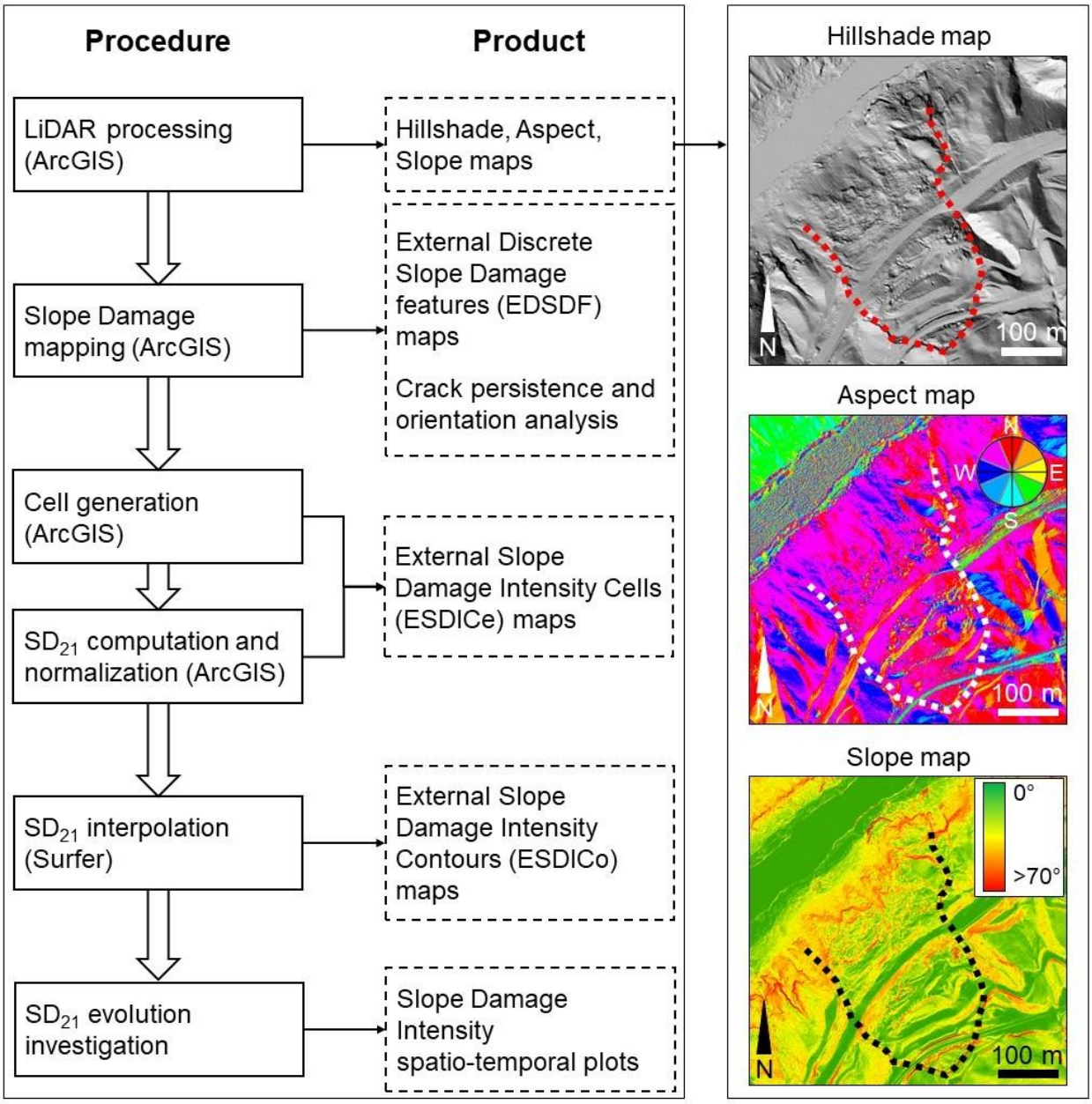

Figure 3: Workflow used for the spatio-temporal slope damage analysis at the Ten Mile Slide. Solid blocks show the processes that have been undertaken; dashed blocks display the map products obtained. Samples of the hillshade, aspect, and slope maps obtained from the January 2017 ALS are also displayed.

4 Spatio-temporal analysis of slope damage at the Ten Mile Slide

4.1. Slope damage mapping and preliminary interpretation

Between 2006 and January 2017, eighteen ALS datasets were collected of the Ten Mile Slide area, which are generally characterized by a sub-metre point spacing. All the datasets were rasterized using CloudCompare 2.9 (CloudCompare, 2017), and Digital Elevation Models (DEMs) were obtained. Using ArcGIS 10.5, aspect, slope, and hillshade maps were created for each DEM. These maps highlight damage features within the datasets, allowing easily identification of cracks, topographic steps, and counterscarps.

In ArcGIS 10.5, damage features (lineaments) were traced as polylines, and based on each DEM an EDSDF map obtained (Figure 4). In general, the minimum crack length that could be mapped was 0.75 m (three times the average resolution of the investigated ALS datasets). Crack width was not addressed in this analysis.

From the analysis of the EDSDF maps it was observed that, since 2006, tensile cracking has predominantly occurred within the eastern portion of the upper slope. In this area, the slope was re-graded in both fall 2010 and summer 2016. Tensile crack accumulation can also be observed in the western part of the domain, in the area immediately above the highway. Between 2006 and 2014, the extension occurring in this area was responsible for a displacement of the highway in excess of 18 m downslope (inset in Figure 5a). In 2015, the retrogression of the slope failure caused the formation of a prominent tension crack above the railway track (Figures 4b and 5b). Since then, minor displacements have also involved the railway embankment.

The slide area may be sub-divided into two slope damage domains, roughly separated by the variation in slope gradient observed along the highway. The upper domain is predominantly characterized by discrete, tensile damage features, such as tension cracks, which form, extend, and coalesce. In the lower domain, slope damage appears to be distributed. Prominent tensile features can be observed in the eastern area, close to the boundary of the slide. Elsewhere, slope damage features can be mostly ascribed to topographic steps and counterscarps.

The damage mapped in the latter ALS dataset was ground-truthed and verified in the course of a site visit in fall 2017, during which the damage features in the upper domain were found to be predominantly extensile in nature. The distributed nature of the slope damage in the lower domain was also confirmed, although discrete tensile cracks were also recognized throughout the domain area (Figure 5c). These observations suggest that a more complex slope failure mechanism affects the development of damage within the lower domain, where discrete, tensile cracks form within a material that is also strongly fragmented and sheared. While the discrete cracks are likely due to the recent slope deformation, it is unclear whether the distributed slope damage formed during the present deformation stage or was inherited from deformation during the older Tunnel earthflow.

Two profiles were traced through the slide area in order to identify the external slope damage and compare it with the slope deformation observed in section for each dataset. Profile 1 is oriented in a north-south direction, roughly parallel with the dip direction of the slope. Profile 2 crosses the slide area in a southwest-northeast direction, in order to investigate the role of the gully along the eastern boundary on the instability (Figure 5a). Figure 6 shows the profiles obtained from two selected ALS datasets, June 2010 and November 2015.

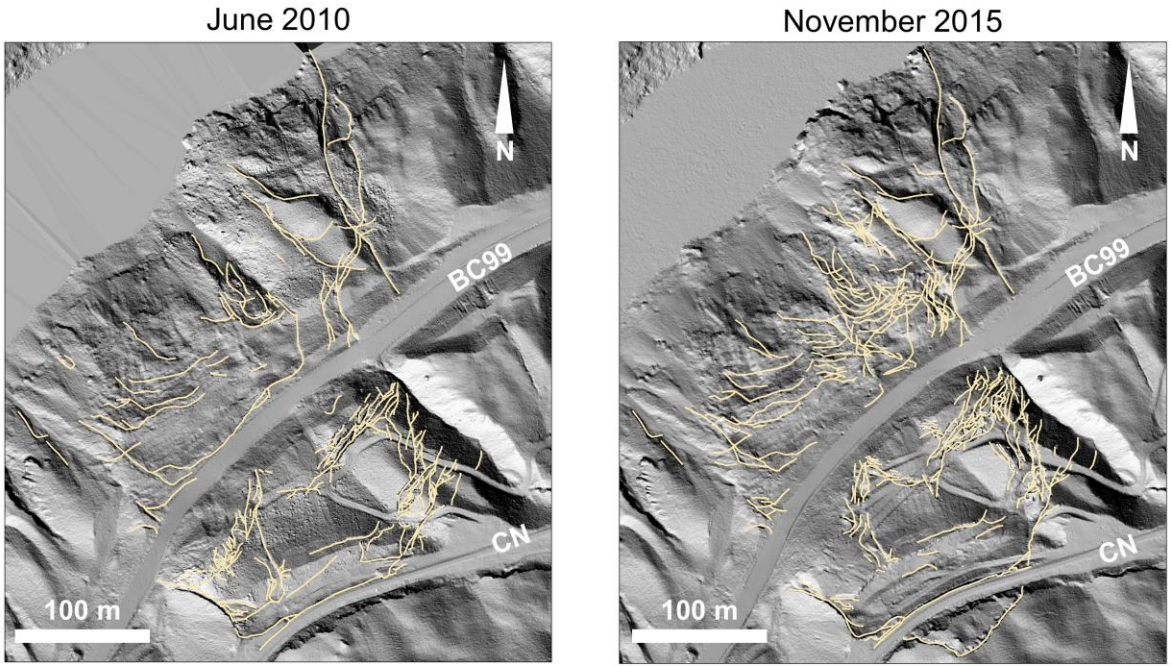

Figure 4: External Discrete Slope Damage Features (EDSDF) map of the Ten Mile Slide site for the June 2010 and November 2015 ALS datasets. Note the increase in cracking throughout the slope, and the formation of the crack above the railway track (indicated as CN in the maps) in 2015.

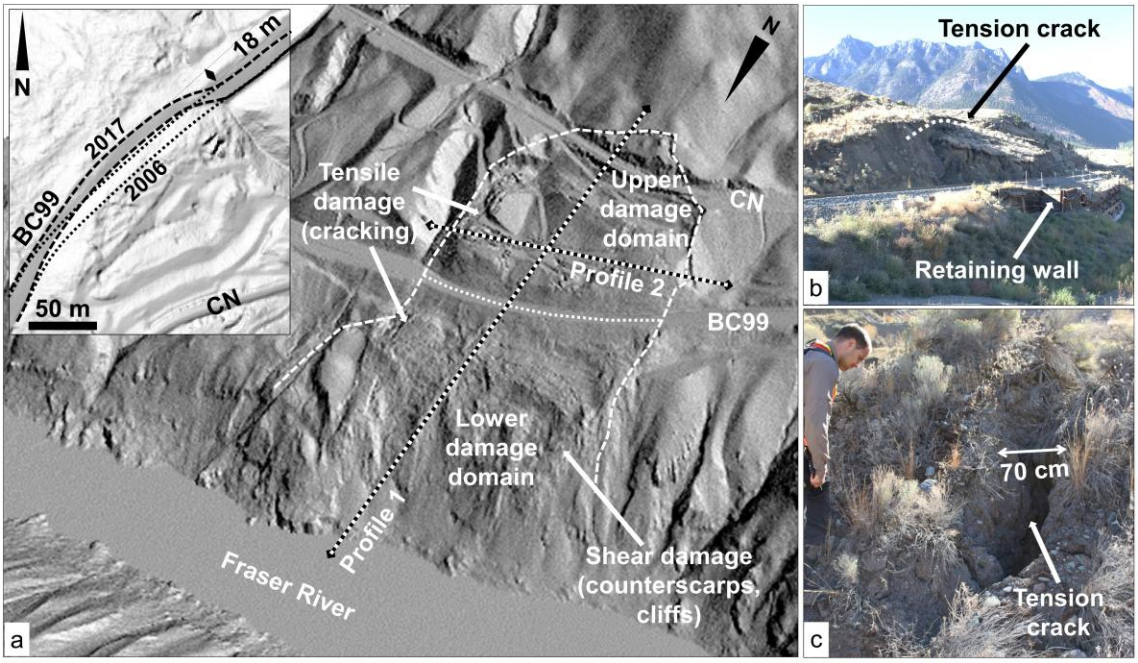

Figure 5: Slope damage domains at the Ten Mile Slide. a: November 2015 ALS dataset of the Ten Mile Slide site. The dashed line outlines the slide area. The dotted line divides the lower and upper damage domains. The dotted, black-white lines indicate the location of the profiles in Figure 6. In the inset, the displacement of the BC99 alignment between 2006 (dotted line) and 2017 (dashed line) is highlighted; b: tension crack at the headscarp of the slide; c: tension crack observed in the lower damage domain.

It was observed that the progressive accumulation of external slope damage, in the form of cracks, cliffs, and scarps, causes the surface roughness to increase. This is particularly evident in the profiles from the June 2010 ALS dataset. In profile 1 a prominent downslope displacement (4 to 5 m) can be observed below the CN railway track (profile 1 in Figure 6a). In the lower slope, the downslope displacement is less obvious. Above the highway cut, surface cracking can be observed that extends to a depth of 3 m. Profile 2 shows high roughness throughout the slide area, and particularly along the eastern boundary of the slide. Here, the slope surface appears to have moved eastward towards and within the gully for 3 to 5 m, suggesting that a lateral deformation occurred, likely governed by this geomorphic feature (profile 2 in Figure 6a). In the November 2015 ALS datasets, profile 1 show the formation of the prominent tension crack behind the CT railway, resulting from the slide retrogression (profile 1 in Figure 6b). From the analysis of profile 2, a limited lateral deformation towards the gully can be observed, which appears to be related to the gradual accumulation of loose material (profile 2 in Figure 6b). It is not clear whether this accumulation is due to lateral expansion or is a result of the slope regrading work performed in 2011.

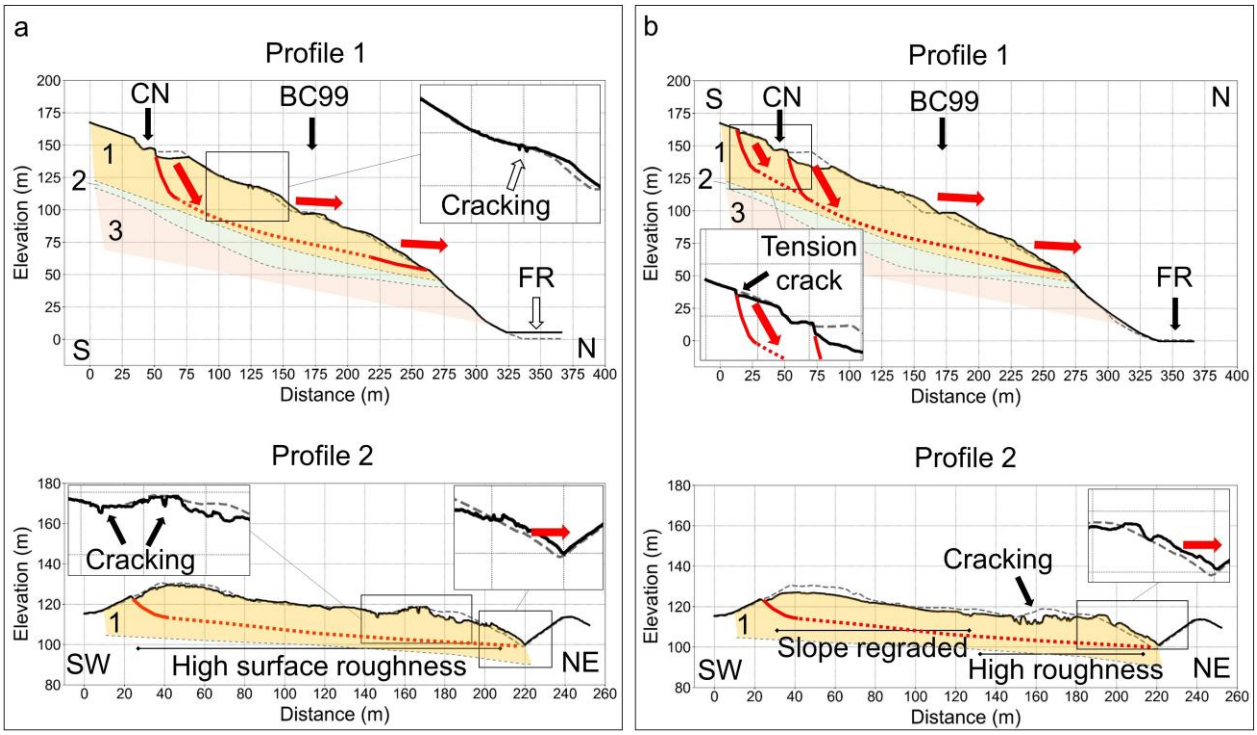

Figure 6: Analysis of the profiles traced in the June 2010 (a) and November 2015 (b) ALS datasets. The 2006 slope surface is shown for reference in the profiles as a dashed, dark grey line. Note the predominant vertical deformation in the upper slope, near the railway track, and the low-angle deformation in the lower part of the slope. Arrows indicate the deformation direction; the location of sliding surfaces within the slide is also shown. Dotted, red line indicate the estimated location of the sliding surface. A simplified stratigraphic succession is also displayed (from Hensold et al., 2017). 1: Tunnel Earthflow; 2: sand anf gravel; 3: undifferentiated glacial sediments; CN: Canadian National Railway track; BC99: highway; FR: Fraser River.

In general, vertical deformation appears to be dominant in the upper part of the slope, whereas in the lower slope, displacements are characterized by a significant sub-horizontal component. This deformation distribution appears to agree with the presence of a low angle sliding surface, as reconstructed from the borehole data (Hensold et al., 2017). The different styles of deformation in the upper and lower slope may be partially controlled by the morphology of the sliding surface, suggesting that the external slope damage distribution and the extent and characteristics of the slope damage domains may also be affected by the rupture surface geometry.

The retrogressive nature of landslides in soil slopes has been investigated by several authors. In particular, Locat et al. (2011) examined from a geotechnical perspective the behavior of landslides in clayey material, where the gradual stress concentration and redistribution causes the progressive retrogression of the landslide. Martin and Stacey (2013) investigated the progressive failure resulting from the stress release in open pit mining in weak rocks, describing the variation in stress and strain occurring within the excavated slope. Poschmann et al. (1983) described the retrogression mechanism that affects rotational slides, observing that the progressive retrogression can result in a "terraced" morphology, with counterscarps in the upper slope and remoulded material in the lower slope. The retrogressive behavior of the Ten Mile Slide was also preliminarily investigated using a conceptual cellular automata model (Mitchell et al., 2018), which has highlighted the potential role of stress redistribution following the formation of slope damage within the topography.

4.2. Persistence and orientation of slope damage features

The persistence of the external slope damage features was investigated by computing the length of all the features in each EDSDF map. The analysis was conducted by considering the upper and lower slope damage domains separately to identify potential differences in accumulation rate between the lower and upper parts of the unstable slope. The cumulative length of the external slope damage features mapped in each EDSDF map is shown in Figure 7. The month that the 2006 and 2009 ALS datasets were collected is not known. In the following analyses it is assumed the flights were performed in June. It was observed that the cumulative external slope damage length has increased continuously in the lower damage domain since 2006, when the first airborne ALS dataset was collected, except for a reduction observed in 2015 due to slope regrading works performed in the area surrounding the highway. On average, the rate of increase of the cumulative external slope damage length over the 2006 to 2017 period is approximately 39 m/month. In the upper damage domain, the cumulative external slope damage length shows a similar increase (34 m/month). These computations do not take into consideration the datasets that show negative changes in cumulative slope damage length, in order to exclude the effects of remediation works. However, it was observed that slope regrading works were generally followed by a spike in the damage accumulation rate, due to the opening of new fractures within a smooth, but still unstable, slope surface. A representative example can be observed in Figure 7, which shows the evolution of the eastern part of the upper damage domain from September 2010, to February 2011, to May 2011. The first dataset shows the slope damage before the beginning of the remediation works. The following datasets highlight the accumulation of external slope damage following the slope regrading works.

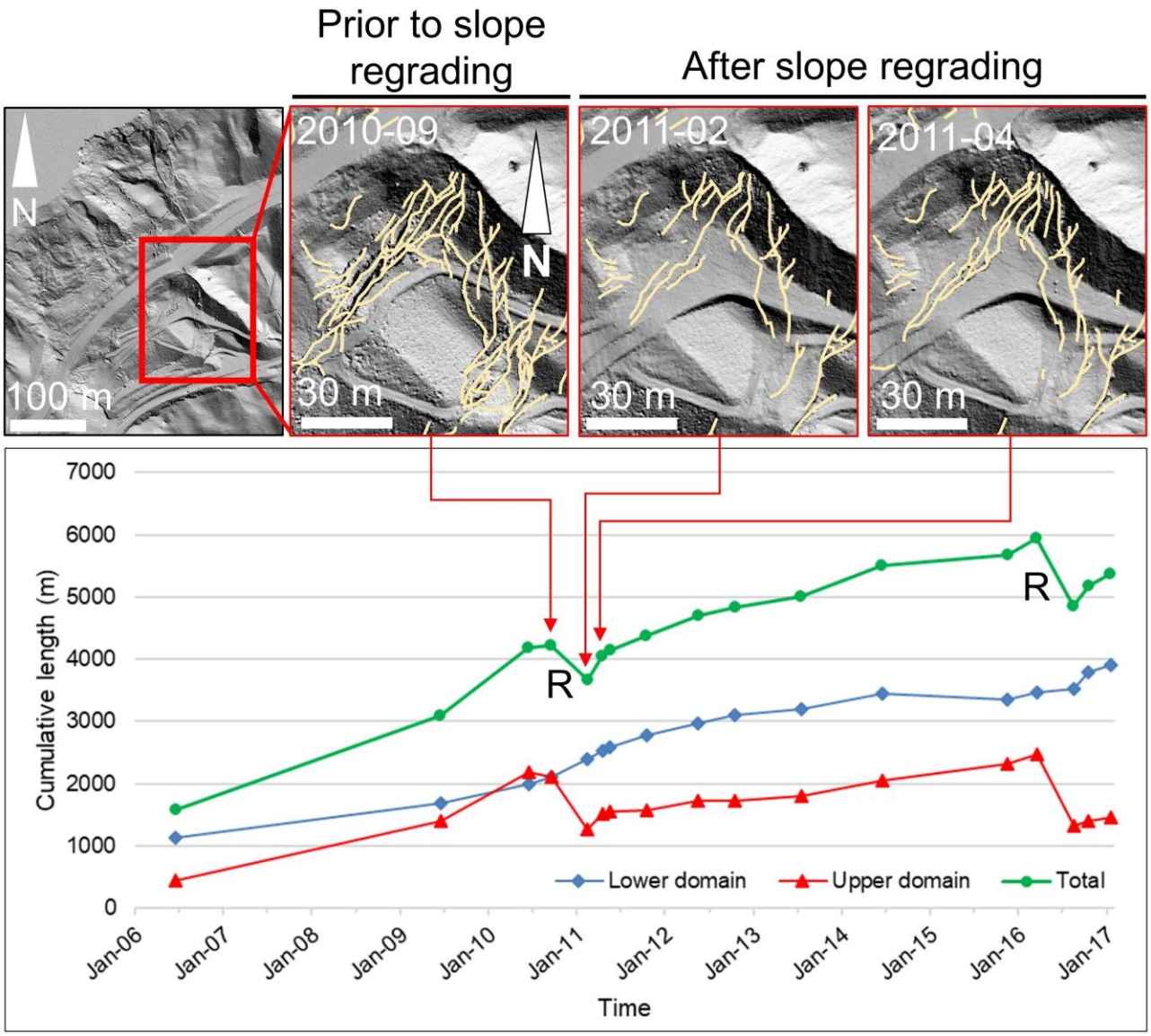

Figure 7: Temporal evolution of the comulative external slope damage length. The graph shows the total comulative crack length computed for each ALS dataset, and the cumulative length in the lower and upper damage domains. R indicate slope regrading work undertaken between ALS surveys. The EDSDF maps highlight the slope damage in September 2010 (before the slope regrading), and the accumulation of external slope damage in the February and May 2011 (after the slope regrading).

Using the EDSDF maps it is possible to extract information on the persistence and orientation of discrete slope damage features. In general, it was observed that the feature persistence distribution follows a log-normal law, and features with persistence lower than 10 m are the most frequently mapped. Figure 8 displays the slope damage persistence frequency distribution for selected ALS datasets, sub-divided between lower and upper slope damage domains. The trend of each crack was also approximately estimated, by measuring the bearing of the segment connecting the start and end point of each feature. This approach was deemed adequate for this analysis in view of the

relatively linear shape of the mapped slope damage features. For each ALS dataset, two rosette diagrams were created, showing the orientation of the features mapped in the lower and upper damage domains. In general, some differences were observed. In the lower damage domain, the predominant trends of slope damage features are oriented in an east-west to northwest-southeast direction. A minor, north-south oriented trend can also be noted (Figure 8). Within the upper damage domain, the slope parallel, east-west trends are overprinted by major north-south to northeast-southwest slope damage trends, which are largely due to the tensile cracking observed in the eastern part of the domain. These trends show a consistent orientation in all the investigated dataset, however, the progressive accumulation of damage throughout the slope, causes them to become less well defined (Figure 8 and 9).

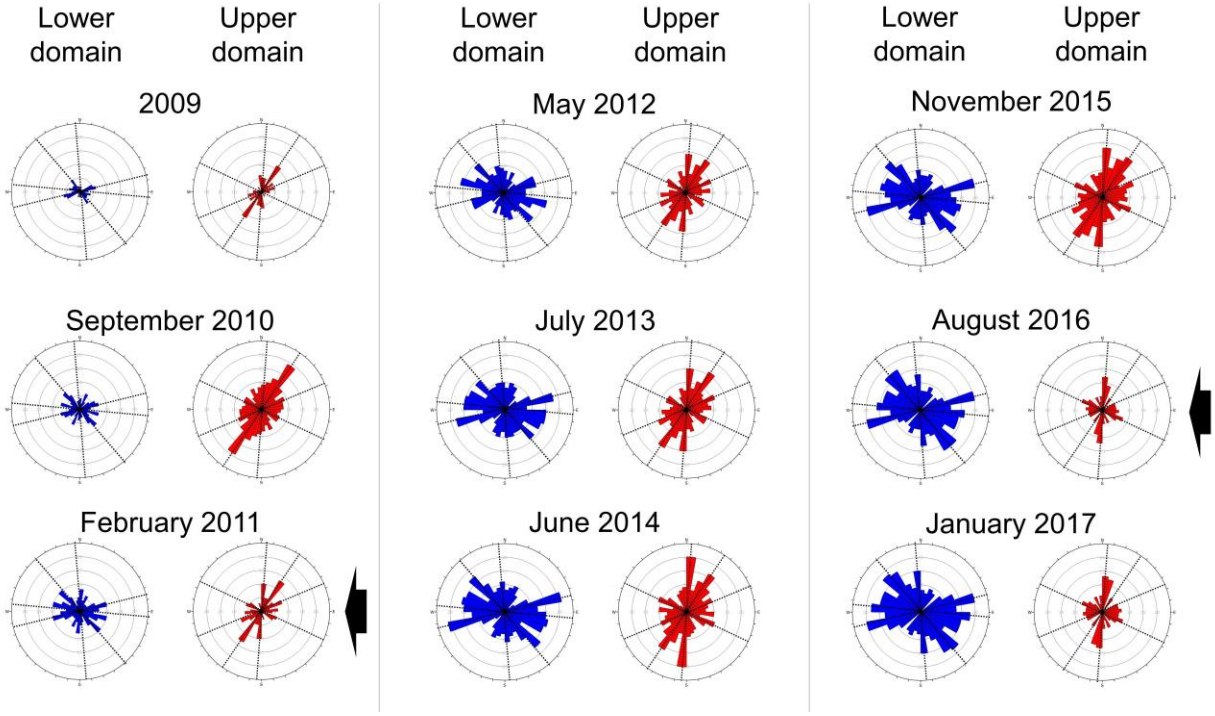

Figure 8 Temporal evolution of slope damage feature orientation for selected ALS datasets. Note the consistency of predominant feature orientation trends across the slide area. East-west to northwest-southeast trends are predominant in the lower slope damage domain (blue rosette plots). In the upper slope damage domain (red rosette plots) the predominant trends are oriented in north-south to northeast-southeast directions. Black arrows mark major regrading works performed in the upper domain, resulting in a local decrease in number of mapped features (cfr. Figure 7).

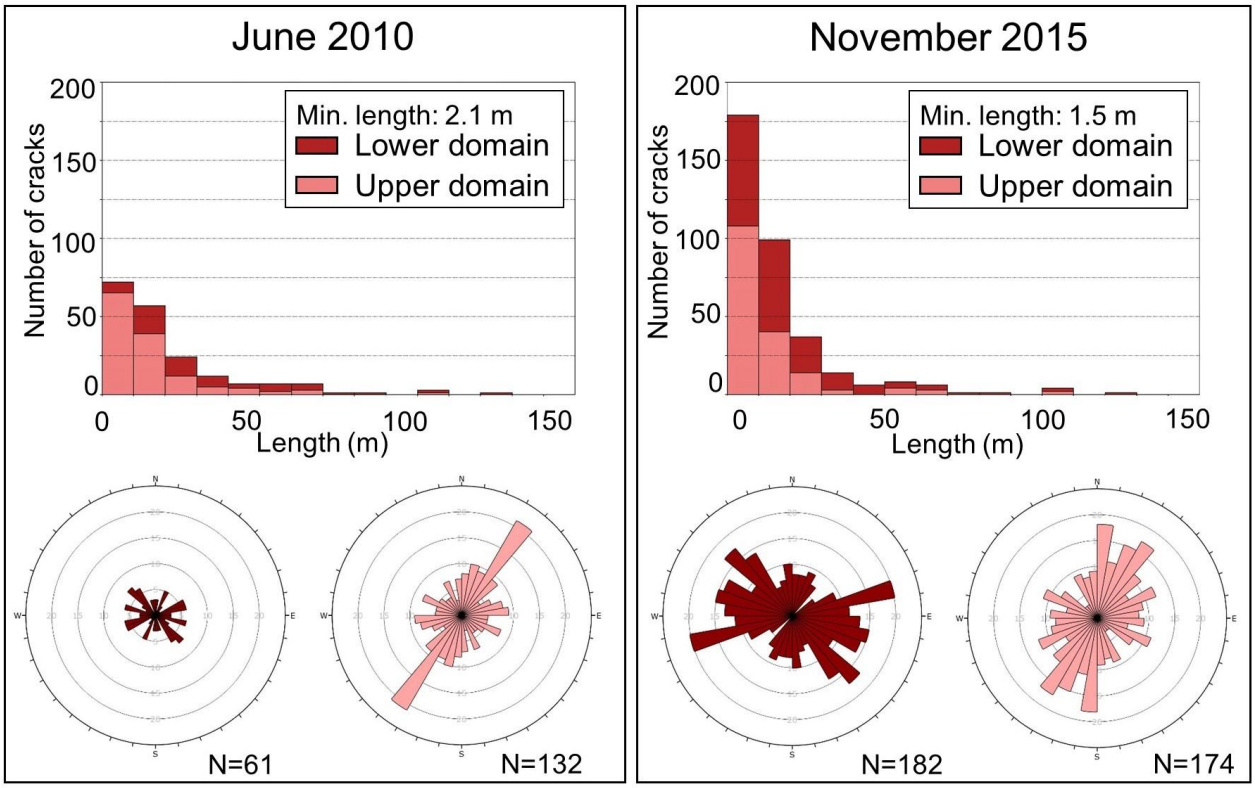

Figure 9: Length and orientation of the external slope damage features mapped at the Ten Mile Slide site. The histograms show the mapping frequency based on the length of the features (bin size is 10 m). The rosette plots shows the orientation of the mapped features Inner circles are every 5 features. In all the plots, dark and light bars relate to the lower and upper damage domain, respectively.

4.3. Slope damage intensity

To obtain indications of the spatial distribution of the slope damage, a damage intensity approach was employed. ESDICe maps were created by dividing the entire slide area into equidimensional cells. The mapped cracks were trimmed within the cell boundaries, and the total length of the cracks was computed for each cell. The SD_{21} value was obtained by dividing the total crack length by the area of the cell. Various cell side sizes were tested, including 10 m, 25 m, and 40 m. A 25 m cell size was found to provide the best compromise between map detail and areal representation (i.e., single damage features do not generate "peaks" in the SD_{21} maps). A 10 m cell size would display a strong correlation between single cracks and peaks in SD_{21} values, therefore lacking the ability to adequately describe the areal slope damage distribution. Conversely, the use of a 40 m cell size resulted in a loss of detail, by smoothing the spatial variability of SD_{21} over a too large area. A normalized SD_{21} value was also calculated, in order to allow a comparison of different SD_{21} maps in the subsequent stages of the analysis. Finally, each cell was colored based on the SD_{21} values (Figure 10a).

For the construction of ESDICo maps, overlapping cells were added to the initial cell assembly in order to increase the data density by four times, and SD_{21} was calculated for each cell. Then, the coordinates of the central point

of each cell were exported, and assigned scalar values corresponding to SD_{21} and normalized SD_{21}. Finally, the point datasets were interpolated in Surfer 14 (Golden Software, 2016), using a Kriging approach (Figure 10b).

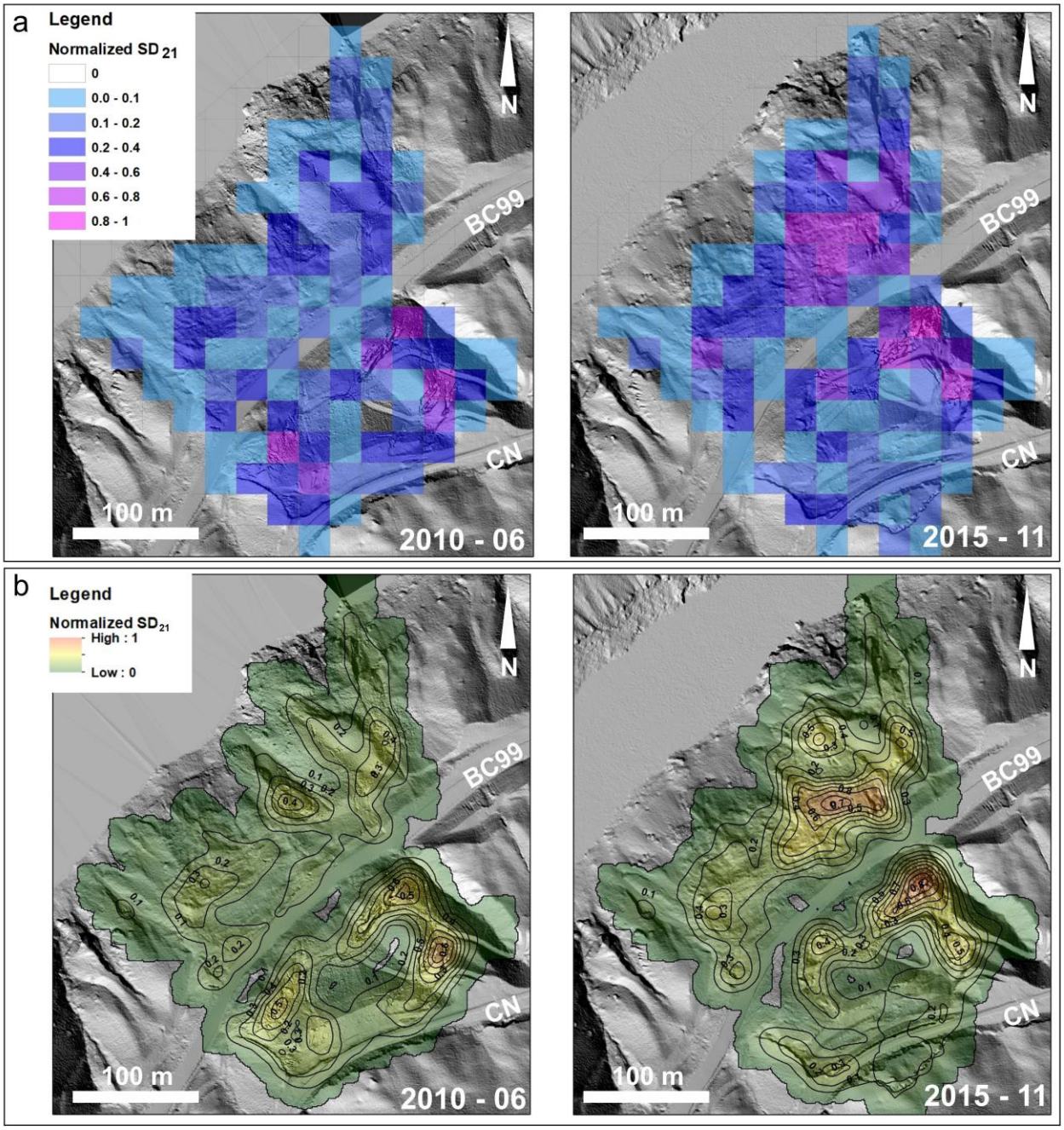

Figure 10: Slope damage intensity maps of the Ten Mile Slide site obtained from the June 2010 and November 2015 ALS datasets. a: normalized External Slope Damage Intensity Cell (ESDICe) maps. Cell size: 25 m; b: normalized External Slope Damage Intensity Contour (ESDICo) maps. Contours every 0.1 of normalized SD_{21} increment.

4.4. Temporal evolution of slope damage intensity

The temporal evolution of the external slope damage was also investigated using a damage intensity approach. A table was created, by indexing the central point of each cell, together with the relative SD_{21} values obtained from the analysis of the EDSDF maps. A Python script was written to interrogate the table, and to plot the changes in SD_{21} computed at any of the 1,833 cells created for each ESDICo map. Selected SD_{21} temporal plots are presented to highlight the areas where external slope damage accumulation has occurred within the upper and lower slope damage domains. SD_{21} has been investigated at two locations within the upper domain; point 1150, along the eastern boundary of the slide area, and point 912, in the central portion of the domain. In the lower domain, SD_{21} was investigated at point 588 and point 874 (Figure 11a). The slope damage time plots are presented in Figures 11b and 11c, and briefly discussed. The evolution of SD_{21} at the selected points was compared with the surface roughness computed using a Vector Ruggedness Method (VRM; Hobson, 1972; Sappington et al., 2007) approach. This method provides a value of ground ruggedness which is independent of the orientation and gradient of the slope.

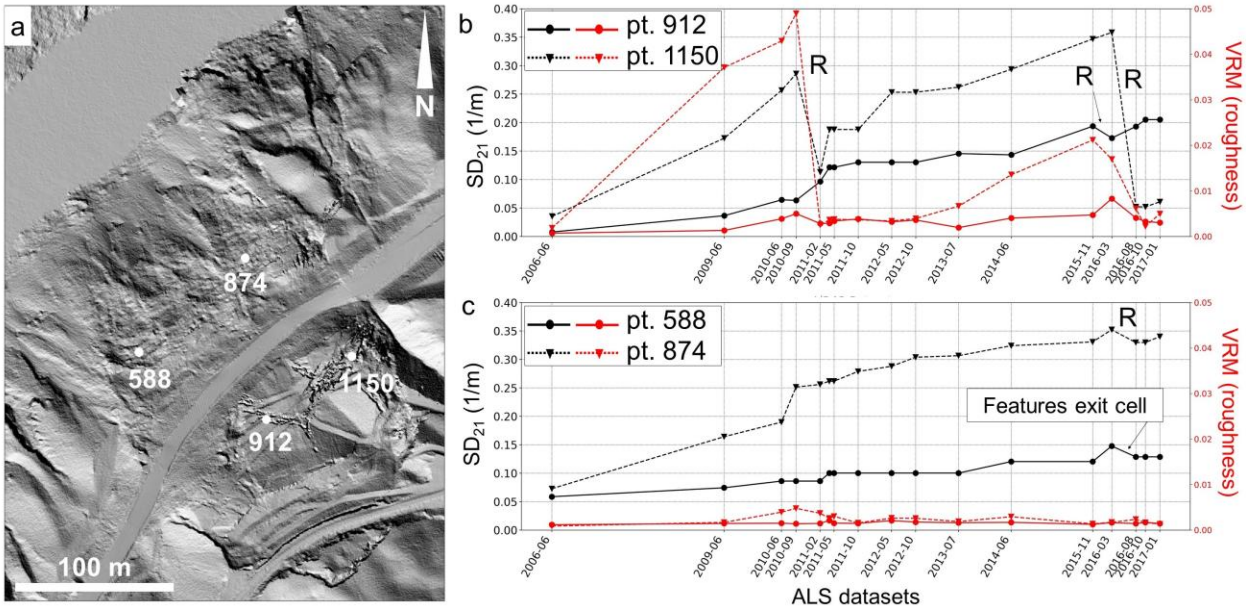

Figure 11: Examples of slope damage temporal plot obtained from the analysis of the Ten Mile Slide. a: location of the investigated points; b: slope damage and surface roughness temporal plots for points 588 (solid line) and 1017 (dashed line) in the lower damage domain; c: slope damage and surface roughness temporal plots for points 912 (solid line) and 1150 (dashed line) in the upper damage domain. Mapped ALS datasets are showed on the x-axis. Rs indicate regressions in slope damage due to regrading of ground surface. Locally, fictitious decreases in slope damage intensity were associated with slope damage features exiting the investigated cell. Note the agreement between slope damage intensity and surface roughness in the upper slope.

4.4.1. Upper domain

The highest values of slope damage intensity in the upper domain are observed along the eastern boundary, at point 1150. Slope cracking in this area has continuously increased since the beginning of the ALS monitoring, with the highest rates of slope damage accumulation occurring between 2006 and 2010 (from 0.04 to 0.29 m^{-1}). On two

occasions, in 2011 and 2016, the slope was re-graded, and the cracks covered (Rs in Figure 11b). As a result, the external slope damage intensity apparently decreased. The maximum slope damage intensity was observed in 2016 (0.36 m^{-1}). At point 912, in the central portion of the upper domain, the observed increase in slope damage intensity is more gradual. Between 2006 and 2017, SD_{21} increased from 0.01 to 0.21 m^{-1}, including an apparent reduction (0.19 to 0.17 m^{-1}) in 2016, due to minor slope regrading. Across the upper domain, a good correlation can be observed between SD_{21} and surface roughness, which displays a more marked rate of increase at point 1150, in the eastern slope, compared to point 915.

4.4.2. Lower domain

Slope damage intensity at Point 588 is characterized by a gradual increase from 0.06 to 0.13 m^{-1} between 2006 and January 2017, with a peak of 0.15 m^{-1} in March 2016. The apparent decrease that followed is due to the displacement of the slide, which caused some of the damage features to exit the cell used to compute the damage intensity value (Figure 11c). Higher values of SD_{21} were observed in the eastern portion of the lower domain, and a peak value was observed at Point 874 (SD_{21} = 0.36 m^{-1}) in the March 2016 ALS dataset. A correlation between high slope damage intensity at point 874 and point 1150, located upslope in the upper domain, was observed. Subsurface data could be used to identify potential structures or features that may be responsible for the damage accumulation along the eastern boundary of the slide area. Across the lower domain, a poorer correlation exists between SD_{21} and surface roughness, which displays a significantly lower variation with time. This may be due to a) the different geomorphic characteristics of the slope damage features in the lower domain, resulting in the formation of smaller undulation compared to the upper slope, or b) a decrease in detail of the ALS datasets, due to the higher slope gradient in the lower domain, which may result in an apparent but fictitious smoother ground surface.

5 Discussion

From analysis of the derived ESDICe and ESDICo maps it is observed that the external slope damage intensity increased between 2006 and 2017. Various regrading works have been undertaken at the site, predominantly in the upper slope damage domain between the highway and CN railway tracks. Between November 2015 and January 2017, a decrease in slope damage intensity has been observed in the eastern part of the upper domain, which occurred due to remediation works covering the existing tension cracks. Conversely, the lower slope displays a continuous increase in slope damage intensity, induced by progressive displacement of the slide.

The Ten Mile Slide has been suggested to be a translational landslide (Hensold et al., 2017). From a kinematic perspective, minimal internal deformation is required for the displacement to occur. This suggests that the progressive increase in external slope damage is strictly related to the differential displacement rates throughout the slide, and the slide retrogression that causes parts of the slopes to gradually become unstable. Lato et al. (2016) highlighted that the slide is divided into blocks that appear to move independently. Such behavior is possibly due to a composite failure mechanism, where steep, pseudo-circular rupture surfaces connect to a basal sliding surface (Figure 12).

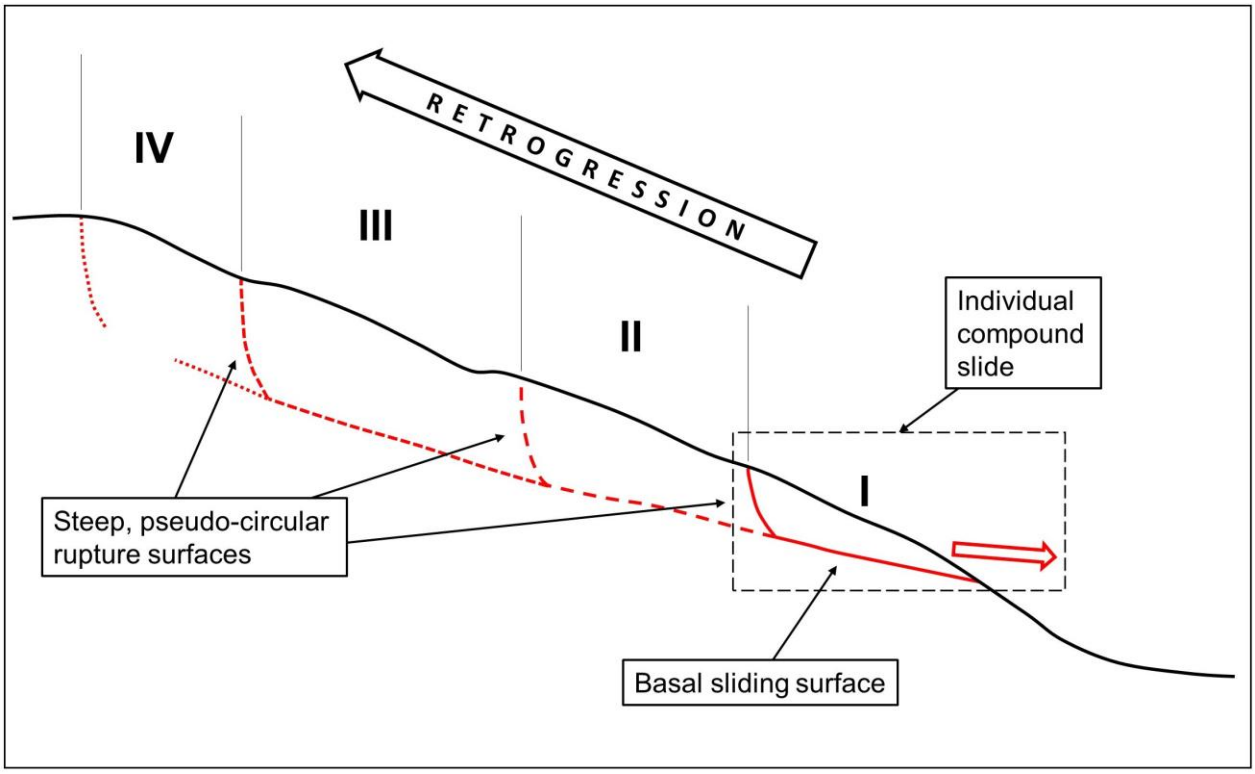

Figure 12: Conceptual model of the evolution of the Ten Mile Slide. Stages I-IV show the progressive retrogression of the slide.

Slope damage intensity does not increase uniformly throughout the entire slide area. In fact, SD_{21} values are consistently higher along the eastern boundary of the slide. The presence of a gully that defines the eastern boundary of the slide area may have an important effect on the slope damage distribution. Such stream incision may enhance kinematic freedom by decreasing the lateral confinement of the slide body in the upper slope (Brideau and Stead, 2011). Lato et al. (2016) observed that the displacement of one of the blocks that they recognized, located in the eastern portion of the upper slope, is directed towards the gully (Figure 13a). This observation is also confirmed by the preliminary analysis of topographic profiles traced across the slope, which shows a lateral deformation of the slide towards this feature. These observations emphasize the role of such stream incision on the spatial distribution of slope damage. The orientation of slope damage features also varies between the upper and lower domains, and the major trends observed in the rosette plots produced appear to agree with the boundaries of the blocks described by Lato et al. (2016), particularly in the upper damage domain (Figure 13b).

The external slope damage time plots also indicate that the increase in damage intensity is particularly marked along the gully that outlines the eastern boundary of the slide area. The temporal damage plot for point 1150 (Figure 11b) shows a rate of slope damage increase not found elsewhere within the slide area, despite the remedial works undertaken in 2010 and 2016. Although it appears that the gully strongly affects the accumulation of slope damage, other factors may play a role in the geomorphic evolution of the slope. For instance, an increase in complexity of the sliding surface morphology may affect the amount internal and external damage required to achieve full kinematic

freedom (Stead and Eberhardt, 2013). Also, the presence of inherited structures within the slope (such as shear zones formed in post-glacial times during the activity of the Tunnel earthflow) may have resulted in localized decrease in the material strength properties and an enhanced intensity of tensile fracturing.

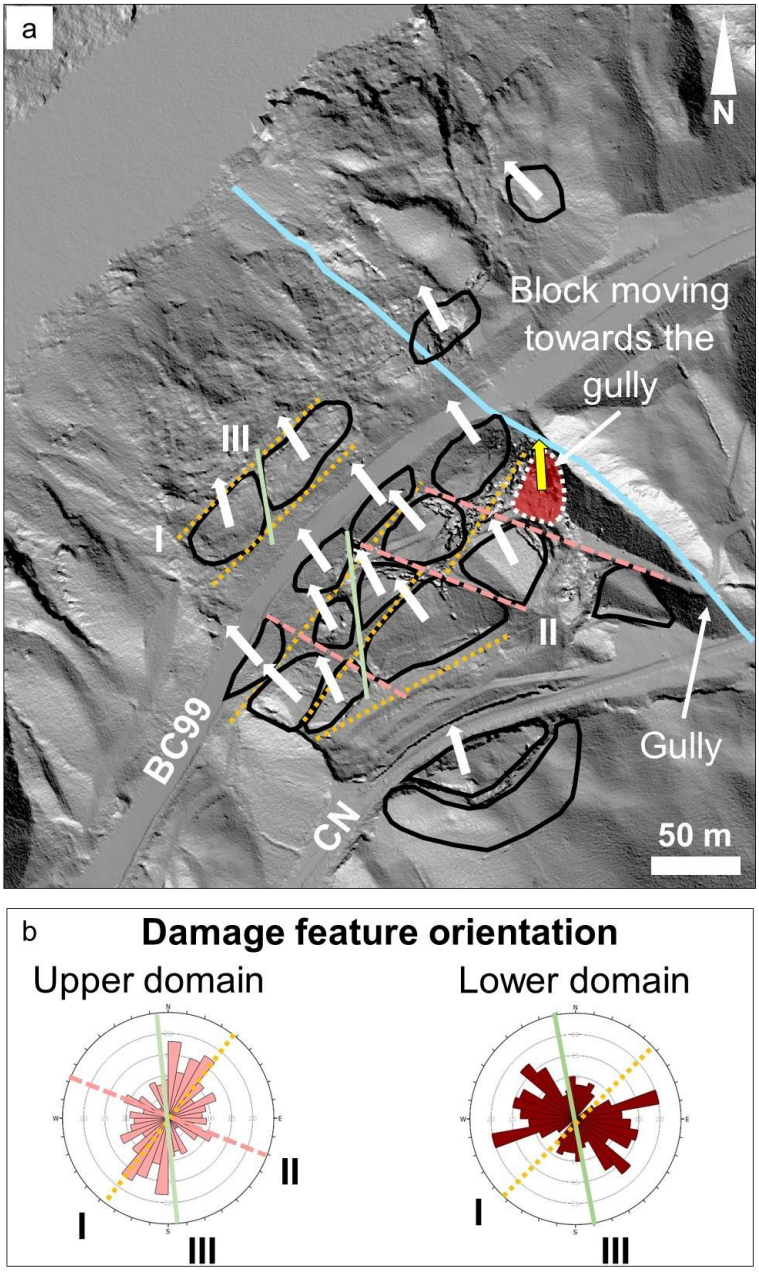

Figure 13: Correlation between slide blocks and slope damage orientation in November 2015 ALS dataset. a: blocks and displacement direction recognized by Lato et al. (2016). The highlighted block is moving towards the gully, suggesting that a lack of lateral confinement may cause the slope damage to increase more than in the rest of the slide area. I, II, and III outline the block boundary trends (figure based on Lato et al., 2016 with permission); b: Rosette plots showing the orientation of slope damage features. Block boundary trends have been overlayed. Note the general agreement with the slope damage orientation in the upper domain.

6 Conclusions

Slope damage mapping undertaken on the ALS datasets available for the Ten Mile Slide site has allowed spatio-temporal characterization of the damage intensity and thereby slope damage evolution. The use of ESDSF, ESDICe, and ESDICo maps has been demonstrated. These proposed slope damage mapping methods provide further insights on the spatial distribution of slope damage within the investigated area. Based on mapping performed on ALS datasets obtained at different times, it has been possible to examine the temporal evolution of slope damage within the slope. The proposed approach could also be applied for the analysis of aerial or satellite imagery. While the described procedure involves the manual mapping of the slope damage features in the ALS datasets, the approach can be easily adapted to include semi-automated or automated feature mapping techniques (including machine learning methods), reducing the level of subjectivity that may be introduced by the surveyor.

The investigation of the spatio-temporal distribution and evolution of slope damage provides an improved understanding of the deformation behavior of unstable slopes. From an engineering practice perspective, identifying areas where external slope damage accumulates may help engineers plan subsequent, more costly investigations (e.g., borehole drilling), and optimize design of new or existent monitoring and early-warning systems. Furthermore, the proposed approach allows for a comparison between slope damage-time plots and other monitoring datasets. Depending on the spatial and temporal resolution of the available datasets, correlation between slope damage and slope displacement, rainfall, temperature, glacial retreat, and seismic activity may be identified, enhancing our understanding of the mechanisms and geological processes underlying the slope instability.

References

Agliardi F, Crosta G, Zanchi A (2001). Structural constraints on deep-seated slope deformation kinematics. Eng Geol 59(1–2): 83–102. https://doi.org/10.1016/S0013-7952(00)00066-1

Agliardi F, Crosta GB, Meloni F, Valle C, Rivolta C. (2013). Structurally controlled instability, damage and slope failure in a porphyry rock mass. Tectonophysics 605: 34–47. https://doi.org/10.1016/j.tecto.2013.05.033

Bovis MJ. (1985). Earthflows in the Interior Plateau, southwest British Columbia. Canadian Geotechnical Journal 22(3): 313–334. https://doi.org/10.1139/t85-045

Brideau MA, Stead D. (2011). The influence of three-dimensional kinematic controls on rock slope stability. In Sainsbury D, Hart R, Detournay C, Nelson M (eds.), Continuum and Distinct Element Numerical Modeling in Geomechanics (Proceedings of the 2nd International FLAC/DEM Symposium), paper 04-05.

Carlà T, Macciotta R, Hendry M, Martin D, Edwards T, Evans T, Farina P, Intrieri E, Casagli N. (2017). Displacement of a landslide retaining wall and application of an enhanced failure forecasting approach. Landslides, 15(3): 489–505. https://doi.org/10.1007/s10346-017-0887-7

Chigira M. (1992). Long-term gravitational deformation of rocks by mass rock creep. Eng Geol 32: 157–184. https://doi.org/10.1016/0013-7952(92)90043-X

Clayton A, Stead D, Kinakin D, Wolter A. (2017). Engineering geomorphological interpretation of the Mitchell Creek Landslide, British Columbia, Canada. Landslides 14(5): 1655–1675. https://doi.org/10.1007/s10346-017-0811-1

CloudCompare 2.9 (2017). CloudCompare 2.9 [GPL software] - Retrieved from http://www.cloudcompare.org/.

de Vilder SJ, Rosser NJ, Brain M. (2017). Forensic analysis of rockfall scars. Geomorphology 295: 202-214.

Dershowitz W, Hermanson J, Follin S, Mauldon M. (2000). Fracture intensity measures in 1-D, 2-D, and 3-D at Aspo, Sweden. In ARMA (ed) Proceedings of the 4th North American Rock Mechanics Symposium. 31 July-3 August 2000. Seattle, WA. Paper ARMA-2000-0849.

Donati D, Stead D, Brideau MA, Ghirotti M. (2017). A remote sensing approach for the derivation of numerical modelling input data: insights from the Hope Slide, Canada. In SAIMM (ed) 'Rock Mechanics for Africa'. Proceedings of the ISRM International Symposium AfriRock Conference. 3-5 October 2017. Paper ISRM AFRIROCK- 2017-066.

ESRI (2017). ArcGIS version 10.5. https://www.esri.com/en-us/home

Fell R, Glastonbury J, Hunter G. (2007). Rapid landslides: the importance of understanding mechanisms and rupture surface mechanics. Q J Eng Geol and Hydrogeol 40(1): 9–27. https://doi.org/10.1144/1470-9236/06-030

Francioni M, Stead D, Clague JJ, Westin A. (2018). Identification and analysis of large paleo-landslides at Mount Burnaby, British Columbia. Environ Eng Geosci 24(2): 221–235. https://doi.org/10.2113/EEG-1955

Gischig VS, Eberhardt E, Moore JR, Hungr O. (2015). On the seismic response of deep-seated rock slope instabilities — insights from numerical modeling. Eng Geol 193: 1–18. https://doi.org/10.1016/j.enggeo.2015.04.003

Glastonbury J, Fell R. (2008). Geotechnical characteristics of large slow, very slow, and extremely slow landslides. Canadian Geotechnical Journal 45(7): 984–1005. https://doi.org/10.1139/T08-021

Golden Software (2016). Surfer version 14.

Havaej M, Stead D, Mayer J, Wolter A. (2014). Modelling the relation between failure kinematics and slope damage in high rock slopes using a lattice scheme approach. In ARMA (ed) Proceedings of the 48th US Rock Mechanics/Geomechanics Symposium. Minneapolis, MN. June 25-28. Paper ARMA-14-7374.

Hensold G, Mitchell A, Porter M, Lato M, McDougall S, Gaib S. (2017). Ten Mile Slide, British Columbia: development of a retrogressive translational earth slide in a post-glacial earthflow deposit. In De Graff JV, Shakoor A (eds) Landslides: Putting Experience, Knowledge and Emerging Technologies into Practice: Proceedings of the 3rd North American Symposium on Landslides. Roanoke, VA: AEG, pp. 316–328.

Hobson, R.D. 1972. Surface roughness in topography: quantitative approach. In: R. J. Chorley (ed) Spatial analysis in geomorphology. Harper and Row, New York, New York, USA, pp. 221–245

Jaboyedoff M, Penna I, Pedrazzini A, Baroň I, Crosta GB (2013). An introductory review on gravitational-deformation induced structures, fabrics and modeling. Tectonophysics, 605: 1–12. https://doi.org/10.1016/j.tecto.2013.06.027

Kromer RA, Hutchinson DJ, Lato M, Gauthier D, Edwards T. (2015). Identifying rock slope failure precursors using LiDAR for transportation corridor hazard management. Eng Geol 195: 93–103. https://doi.org/10.1016/j.enggeo.2015.05.012

Lato M, Porter M, Hensold G, McDougall S, Kromer R, Gaib S. (2016). Understanding landslide movement and kinematics with airborne LiDAR. In CGS (ed) Proceedings of 69th Canadian Geotechnical Society Conference, GeoVancouver 2016. Vancouver, BC. 2-5 October 2016. Paper 4115.

Leshchinsky B. (2016). Contour Connection Method: A Semi-automated method for hazard mapping using LiDAR. In: Aversa S, Cascini L, Picarelli L, Scavia C (eds) Landslides and Engineered Slopes. Experience, Theory and Practice: Proceedings of the 12th International Symposium on Landslides. Napoli, Italy, 12-19 June 2016: CRC Press, pp. 1267-1273.

Locat A, Lerouil S, Bernaden S, Demers D, Jostad HP, Ouehb L. (2011). Progressive failures in eastern Canadian and Scandinavian sensitive clays. Canadian Geotechnical Journal, 48. pp. 1696-1712. https://doi.org/10.1139/t11-059

Macciotta R, Rodriguez J, Hendry M, Martin CD, Edwards T, Evans T. (2016). The 10-mile Slide north of Lillooet, British Columbia – history, characteristics and monitoring. In De Graff JV, Shakoor A (eds) Landslides: Putting Experience, Knowledge and Emerging Technologies into Practice: Proceedings of the 3rd North American Symposium on Landslides. Roanoke, VA: AEG, pp. 937–948.

Martin CD, Stacey PF (2013). Pit slopes in weathered and weak rocks. In Dight PM (ed) Proceedings of the 2013 International Symposium on Slope Stability in Open Pit Mining and Civil Engineering. Perth, September 25-27. pp. 3-28. Keynote address.

Mathews WH, McTaggart KC (1978). Hope Rockslides, British Columbia, Canada. In Voight B (ed). Rockslides and Avalanches, 1: 259–275.

Mitchell A, Whadcoat S, McDougall S, Porter M, Gaib S. (2018). Application of a cellular stress transfer model for retrogressive landslides. In CGS (ed) Transportation Geotechnique - Moving Forward. Proceedings of the 71st Canadian Geotechnical Conference GeoEdmonton 2018. Edmonton, September 23-26. Paper 225.

Monger JWH, McMillan WJ (1984). Bedrock geology of Ashcroft (92 I) map area. In Ryder GM (ed) Terrain inventory and quaternary geology Ashcroft, British Columbia, Geological Survey of Canada. Paper no. 74-49. Retrieved from: https://geoscan.nrcan.gc.ca/. GEOSCAN ID 109031.

Piteau DR, Ylrea FH, Blown IG (1978). Downie Slide, Columbia River, British Columbia, Canada. In Voight B (ed) Rockslides and avalanches, Volume 1: 365–392.

Poschmann AS, Klassen KE, Klugman MA, Goodings D. (1983). Slope stability study of the South Nation River and portions of the Ottawa River – Miscellaneous paper 112. Ontario Geological Survey.

Preisig G, Eberhardt E, Smithyman M, Preh A, Bonzanigo L. (2016). Hydromechanical rock mass fatigue in deep-seated landslides accompanying seasonal variations in pore pressures. Rock Mech Rock Eng 49(6): 2333–2351. https://doi.org/10.1007/s00603-016-0912-5

Roberti G, Ward B, van Wyk de Vries B, Friele P, Perotti L, Clague JJ, Giardino M. (2018). Precursory slope distress prior to the 2010 Mount Meager landslide, British Columbia. Landslides 15(4): 637–647. https://doi.org/10.1007/s10346-017-0901-0

Stead D, Eberhardt E. (2013). Understanding the mechanics of large landslides. Italian Journal of Engineering Geology and Environment - Book Series (6): 85–112.

Stead D, Wolter A. (2015). A critical review of rock slope failure mechanisms: the importance of structural geology. J Struct Geol 74: 1–23. https://doi.org/10.1016/j.jsg.2015.02.002

Stumpf A, Malet JP, Kerle N, Niethammer U, Rothmund S. (2013). Image-based mapping of surface fissures for the investigation of landslide dynamics. Geomorphology 186: 12-27.

Williams JG, Rosser NJ, Hardy RJ, Brain MJ, Afana AA (2018). Optimising 4-D surface change detection: An approach for capturing rockfall magnitude frequency. Earth Surf Dyn 6(1): 101–119. https://doi.org/10.5194/esurf-6-101-2018